Propagation of a Gaussian-profile laser beam in nematic liquid crystals and the structure of its nonlinear diffraction rings

J. J. Wu

Institute of Electronics, National Chiao Tung University, Hsinchu, Taiwan 30050, China

Shu-Hsia Chen, J. Y. Fan, and G. S. Ong

Institute of Electro-Optical Engineering, National Chiao Tung University, Hsinchu Taiwan 30050, China

Received April 26, 1989; accepted October 25, 1989

We present experimental results on and a theoretical explanation of the laser- and electric-field-induced diffraction effect in both homeotropic and homogeneous nematic liquid-crystal (NLC) films. The diffraction effect is due to the Gaussian profile of a laser beam propagating in the liquid crystal. Many diffraction ring patterns under different electric and optical fields are compared and are analyzed. Some novel phenomena have been discovered. We have found that the diffraction ring pattern at a high electric field is much different from that at a low electric field. Rings in a pattern should be asymmetrical to one axis, and the outer ring interval should be wider. For the homogeneous NLC film it is possible that a second set of diffraction rings may occur when the electric field or the maximum optical field is larger than the tricritical field. The numerical result for the deformed wave-front profile of a Gaussian-profile laser beam passing through the NLC film is calculated. The results can explain these novel phenomena of diffraction ring structures.

I. INTRODUCTION

In the past few years considerable attention has been paid to the electromagnetic-field-induced refractive-index change in nonlinear media such as nematic liquid crystals (NLC's).[1-3] Because of its large molecular anisotropy and the strong correlation among the molecules, it is well known that the director, i.e., the average molecular orientation of the liquid-crystalline material, can be easily reoriented by a static electric, magnetic,[4] or optical field, and the birefringence of the sample would change accordingly. This is referred to as the Freedericksz transition. Electrically controlled birefringence has since been used for light valves and in other applications.[5] Studies of optical-field-induced molecular reorientations of the nematic phase of liquid crystals have also revealed interesting nonlinear effects of both fundamental and applied significance.[6] The optical-field-induced Freedericksz transition and associated nonlinear-optical effects in a NLC film, such as self-focusing, degenerate wave mixing, and optical bistability, have been studied extensively recently.[7-9] Most of these effects can be achieved with lasers of moderate output power.

In particular, interesting nonlinear-optical propagation effects, e.g., far-field diffraction rings,[10-12] have been observed and applied as a measurement method in experiments. This phenomenon has been described as the spatial analog of the well-known self-phase modulation of light as the laser beam traverses the sample. The diffraction effect is shown to be further enhanced or suppressed by biasing the sample with a quasi-static electric field. By counting the number of diffraction rings, it was also recently shown theoretically and experimentally that intrinsic optical bistability in both homeotropically and homogeneously aligned NLC cells can be enhanced or suppressed by a low electric or magnetic field. In addition, the electric bistability can be enhanced by an optical field.[13-22]

The characteristics and the theory of the diffraction effect in NLC films have been treated briefly by several researchers in various contexts.[8,11,23-28] Their theories generally matched their experimental results well. However, these observations have not been reported in detail. Some novel phenomena cannot be explained by using these theories. A more exact description of the transverse spatial dependence of both the laser beam and the nematic reorientation is required.

In this paper we present results of a detailed investigation of electric- and optical-field-induced birefringence and diffraction effects in both homeotropically and homogeneously aligned thin ROTN-200 NLC films, and we propose a new wide-ranging viewpoint of these phenomena. In the Discussion (Section 4) we also predict some phenomena that should be induced by diffraction effects but have not been observed in experiment. In Section 2 we briefly state the essential results from the theory for field-induced molecular reorientation angles and birefringence. In Section 3 our experimental method is outlined and the experimental results are summarized. In Section 4 we discuss the new phenomena seen in our experiment and make some further predictions

0740-3224/90/061147-11$02.00

for the diffraction ring patterns. In particular, we report for the first time (to our knowledge) a novel second set of diffraction rings for a normally incident laser beam.

2. THEORY

Homeotropic Nematic Liquid-Crystal Film

Let us first consider a homeotropically aligned nematic film of thickness d confined between the planes $z = 0$ and $z = d$ in a Cartesian coordinate system as shown in Fig. 1(a). In addition to a normally incident and linearly polarized infinite plane wave with constant intensity I, an electric potential V is applied along the surface normal. Assuming that $n_\parallel > n_\perp$ and $\epsilon_\parallel > \epsilon_\perp$, where n and ϵ denote the refractive indices and dielectric constants, respectively, and refer to directions parallel and perpendicular to the director, the optical field will orient the molecule along the y axis, and the electric field will orient the molecule along the z axis and hence suppress the optical-orienting effect. The orientation of the NLC's director $\hat{n} = (0, \sin\theta, \cos\theta)$ can be described by the angle $\theta(z)$ between the director and the z axis.

In general, the total free-energy density F, which consists of the elastic deformation, optical field, and electric field energy densities, can be expressed in terms of $\theta(z)$. Variation of the total free energy leads to a Euler equation $\theta(z)$.

Owing to the symmetry of the problem, one can look for symmetrical solutions satisfying $\theta(z) = \theta(d - z)$. Using the rigid boundary condition, the following equation can be derived from the Euler equation as[14,15,18]

$$\int_0^{\theta_m} \left\{ \frac{1 - k\sin^2\theta}{n(\theta_m) - n(\theta) - R[P(\theta_m) - P(\theta)]} \right\}^{1/2} d\theta = \pi \left(\frac{p}{2n_\perp u} \right)^{1/2}, \tag{1}$$

where $\theta_m = \theta(z = d/2)$, $k = 1 - k_{11}/k_{33}$, k_{11} is the splay elastic constant, k_{33} is the bend elastic constant,

$$n(\theta) = n_\perp/(1 - u\sin^2\theta)^{1/2}, \qquad u = 1 - {n_\perp}^2/{n_\parallel}^2,$$
$$R = c{D_z}^2/(8\pi\epsilon_\parallel I), \qquad P(\theta) = 1/(1 - w\sin^2\theta),$$

$w = 1 - \epsilon_\perp/\epsilon_\parallel$, c is the speed of light in vacuum, D_z is the z component of the electric displacement, and $p = I/I_0$ is the normalized optical intensity, where $I_0 = (ck_{33}/n_\perp u)/(\pi/d)^2$. In addition, R is related to the applied voltage V through

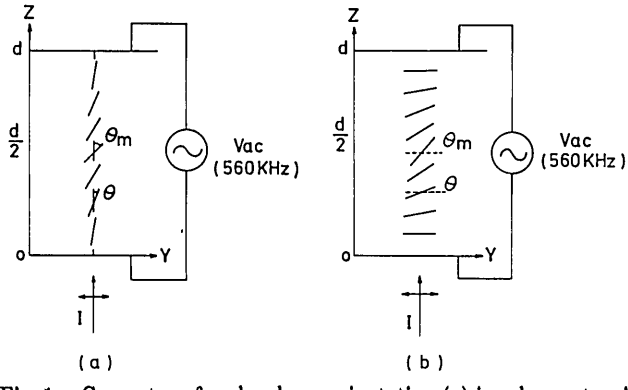

Fig. 1. Geometry of molecular reorientation (a) in a homeotropic NLC cell and (b) in a homogeneous NLC cell, with optical and electric fields.

$$V = \int_0^d E_z dz = \int_0^d D_z/[\epsilon_\parallel(1 - w\sin^2\theta)]dz,$$

from which one can obtain

$$\int_0^{\theta_m} P(\theta) \left\{ \frac{1 - k\sin^2\theta}{n(\theta_m) - n(\theta) - R[P(\theta_m) - P(\theta)]} \right\}^{1/2} \times d\theta = \frac{\pi}{2} \left(\frac{1}{wR} \right)^{1/2} r, \tag{2}$$

where $r = V/V_0$ is the normalized electric potential, V is the electric potential, and $V_0 = 2\pi[\pi k_{33}/(\epsilon_\parallel - \epsilon_\perp)]^{1/2}$. From Eqs. (1) and (2), a linear relation between I/I_0 and $(V/V_0)^2$ is given as

$$I/I_0 = 1 + (V/V_0)^2. \tag{3}$$

The tricritical voltage and tricritical intensity are

$$V_{Tc} = V_0\,|4(1 - k - 9u/4)/9u - 4w)|^{1/2} \tag{4}$$

and

$$I_{Tc} = I_0[4(1 - k - w)/(9u - 4w)]. \tag{5}$$

When $V > V_{Tc}$ or $I > I_{Tc}$, the Freedericksz transition is first order; otherwise it is second order. Using Eqs. (1) and (2), the unknown parameters θ_m and R can be derived as functions of p and r. The exact solution for the maximum deformation angle θ_m for a homeotropic NLC at a given p and r is then described by Eqs. (1) and (2). The induced phase shift of the extraordinary ray in the medium can be expressed as $\Delta\Phi = (2\pi/\lambda)\int_0^d [n_\perp - n(\theta)]dz$, where λ is the wavelength of the light. Following Ong's derivation,[14] the exact solution for $\Delta\phi$ induced by an infinite plane wave is given by

$$\Delta\phi = -\frac{2d}{\lambda} \left(\frac{2n_\perp u}{p} \right)^{1/2} \int_0^{\theta_m} n(\theta) \times \left\{ \frac{1 - k\sin^2\theta}{n(\theta_m - n(\theta) - R[P(\theta_m) - P(\theta)]} \right\}^{1/2} d\theta + \frac{2\pi n_\perp d}{\lambda}. \tag{6}$$

This is an exact solution of the induced phase shift for a normal incident infinite plane wave on the hometroptic NLC film.

However, in reality, the light source does not emit an infinite plane wave. The laser intensity profile is not uniform but has a Gaussian distribution. In order to obtain the numerical results, we calculated the induced phase shift in a straightforward way by using a Gaussian-beam approximation, which assumes that the radii of the beams (as well as their Gaussian profiles) change very little as the beams pass through each nonlinear layer and assumes that the nonlocal effect is not significant. The corresponding phase shift $\Delta\phi$ at any transverse position $\rho = (x^2 + y^2)^{1/2}$ in the beam can be obtained. When the relation between $\Delta\phi$ and ρ is examined, a numerical result is obtained that shows that the plane wave of a laser beam is deformed when it passes through the homeotropic NLC film. Because of the deformation of the wave front, the diffraction rings can be seen in the far-field pattern.[20–22] Here it should be noted that the actual nonlocal effect is not negligible. Using one constant approximation and neglecting the electric field effect, Khoo *et al.* have reported[26] that the threshold intensity will increase to ap-

proximately 2.4 times I_0 for the case of a laser beam size ω_0 equal to the sample thickness d; but in our experiment, both the electric and the optical fields are used. To explain our novel experimental phenomena without too complicated a numerical calculation, we use Ong's exact solution for an infinite plane wave and neglect the nonlocal effect in order to simplify the problem. This is reasonable because we use only low intensity and the induced phase shift $\Delta\phi/2\pi \leq 9$, i.e., $\theta_m \ll 1$. If $\theta_m \ll 1$, the nonlocal effect can change the value of I_{th} but cannot greatly affect the shape of the diffraction ring pattern.

The explanation for the formation of the diffraction rings as follows.[12] Above the threshold for the Freedericksz transition, the optical field reorients the director of molecular alignment in the y–z plane throughout the medium. This leads to a local refractive-index change $\Delta n(\rho, z)$ in the medium seen by the laser and a corresponding phase shift $\Delta\phi(\rho)$. For a single-transverse-mode laser, we may expect that $\Delta\phi(\rho)$ is cylindrically symmetric in the form of a concavity with its minimum at $\rho = 0$. We assume, for simplicity, that the relative induced phase shift

$$\Delta\Psi(\rho) = \Delta\phi(\rho = \rho) - \Delta\phi(\rho \to \infty) = \Delta\Psi_0 \exp(-2\rho^2/a^2, \quad (7)$$

where a is a constant. Then, as is seen in Fig. 2, for each point, say ρ_1, on the $\Delta\Psi(\rho)$ curve, there always exists another point ρ_2 with the same slope. Since $d\Delta\Psi/d\rho = k_\rho$, where k_ρ is the component of the wave vector in the $\hat{\rho}$ direction, the radiation fields from the regions around ρ_1 and ρ_2 have the same wave vector and can interfere. Maximum constructive or destructive interference occurs when $\Delta\Psi(\rho_1) - \Delta\Psi(\rho_2) = m\pi$, m being an even or odd integer, with the resulting appearance of diffraction rings. Thus, if $\Delta\Psi_0 \gg 2\pi$, multiple diffraction rings are expected, and the total number of rings N can be estimated from the relation

$$N \simeq \Delta\Psi_0/2\pi. \quad (8)$$

The outermost ring should come from radiation from the region ρ near the inflection point on the $\Delta\Psi(\rho)$ curve, and its half-cone angle β_m can be calculated from

$$\beta_m \simeq \left(\frac{d\Delta\Psi}{d\rho}\right)_{\max} \Big/ \frac{2\pi}{\lambda} = \left[\frac{d}{d\rho}\left(\frac{\Delta\Psi}{2\pi}\lambda\right)\right]_{\max}. \quad (9)$$

In fact, there is a more precise equation described in the paper of Khoo *et al.*[27] to calculate the diffraction phenomena. They use a straightforward application of Kirchhoff's diffraction integral to yield the intensity distribution at the observation plane $Z = z + d$:

$$I(\rho_1, Z) = (2\pi/\lambda Z)^2 I_0 \times \left| \int_0^\infty \rho d\rho J_0(2\pi\rho\rho_1/\lambda Z) \exp(-2\rho^2/\omega_0^2) \exp[-i(\phi_D + \phi_{\text{NL}})] \right|^2,$$

where ϕ_D is the diffractive phase and ϕ_{NL} is the nonlinear-(intensity-) dependent phase. The value of ϕ_D is given as[27]

$$\phi_D = \frac{2\pi}{\lambda}\left(\frac{\rho^2}{2Z} + \frac{\rho^2}{2\mathcal{R}}\right),$$

where $\mathcal{R}$ is the radius of wave curvature. In our experiment we put our sample at the focus, so that $\mathcal{R} = \infty$ and $\phi_D = 0$. However, for ϕ_{NL}, Khoo *et al.* give the approximate expression[27]

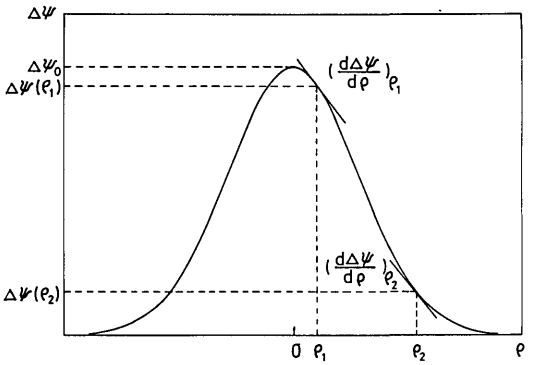

Fig. 2. Relation of the wave-front deformation and the diffraction rings.

$$\phi_{\text{NL}} = k\bar{n}_2 d I_0 \exp\left(-\frac{2\rho^2}{\omega_0^2}\right),$$

where $\bar{n}_2$ is the nonlinear refractive-index coefficient and $k = 2\pi/\lambda$. As a matter of fact, ϕ_{NL} is not so simple as the expression of Khoo *et al.*, because ϕ_{NL} is not proportional to $I_0 \exp[-(2\rho^2/-\omega_0^2]$ and $\bar{n}_2$ is dependent on the optical and the electric field. Even for the simplest case, a normal-incident infinite plane wave, the exact solution of ϕ_{NL} has the complicated form displayed in Eq. (6). In our experiment, the incident light is a finite-sized beam and, as will be explained in our discussion, the light beam and the material's nonlinear index of refraction will affect each other. This is why it is almost impossible to get an exact solution even by a numerical method. For this reason, we choose expressions (7)–(9), which are simple but maintain the physical meaning. We find that our theoretical and numerical results can explain the experimental phenomena qualitatively.

Homogeneous Nematic Liquid-Crystal film

Let us now consider the homogeneous NLC as shown in Fig. 1(b). An electric field of potential V is applied along the surface normal, and a linearly polarized infinite plane wave of constant intensity I polarized parallel to the y axis is incident normal to the NLC film. The orientation is described by the director $\hat{n} = (0, \cos\theta, \sin\theta)$, where $\theta(z)$ is given by the equations[17,18]

$$\int_0^{\theta_m} \left\{\frac{1 - k\sin^2\theta}{n(\theta_m) - n(\theta) - R[P(\theta_m) - P(\theta)]}\right\}^{1/2} d\theta = \pi\left(\frac{p}{2n_\parallel u}\right)^{1/2}, \quad (10)$$

$$\int_0^{\theta_m} P(\theta)\left\{\frac{1 - k\sin^2\theta}{n(\theta_m) - n(\theta) - R[P(\theta_m) - P(\theta)]}\right\}^{1/2} \times d\theta = \frac{\pi}{2}\left(\frac{1}{wR}\right)^{1/2} r, \quad (11)$$

where $k = 1 - k_{33}/k_{11}$, $n(\theta) = n_\parallel/(1 + u\sin^2\theta)^{1/2}$, $u = n_\parallel^2/n_\perp^2 - 1$, $R = cD_z^2/(8\pi\epsilon_\perp I)$, $D_z = \epsilon_\perp(1 + w\sin^2\theta)E_z$, $P(0) = 1/(1 + w\sin^2\theta)$, $w = \epsilon_\parallel/\epsilon_\perp - 1$, $p = I/I_0$, $I_0 = (ck_{11}/n_\parallel u)/(\pi/d)^2$, $r = V/V_0$, and $V_0 = 2\pi[\pi k_{11}/(\epsilon_\parallel - \epsilon_\perp)]^{1/2}$. From Eqs. (10) and (11), the tricritical voltage V_{Tc} and tricritical intensity I_{Tc} can be obtained, and the linear relation between I/I_0 and $(V/V_0)^2$ can be expressed as

$$I/I_0 + 1 = (V/V_0)^2. \tag{12}$$

Again, when $V > V_{Tc}$ or $I > I_{Tc}$, the Freedericksz transition is first order; otherwise it is second order. The induced phase shift $\Delta\phi$ of the extraordinary ray in the NLC film with thickness d can be expressed as

$$\Delta\phi = \frac{2d}{\lambda}\left(\frac{2n_{\parallel}u}{p}\right)^{1/2}\int_0^{\theta_m} n(\theta)$$

$$\times\left\{\frac{1 - k\sin^2\theta}{n(\theta_m) - n(\theta) - R[P(\theta_m) - P(\theta)]}\right\}^{1/2} d\theta - \frac{2\pi n_{\parallel} d}{\lambda} \tag{13}$$

The relative induced phase shift $\Delta\Psi$ of of the beam is then given by $\Delta\Psi(\rho) = \Delta\phi(\rho = \rho) - \Delta\phi(\rho \to \infty)$, as in the homeotropic case.

3. EXPERIMENT

The experiment used a cw Ar^+ laser focused to a diameter of 300 μm at the ROTN-200 sample. The sample cell was 250 μm thick with the windows coated with dimethyl octadecyl-3-(trimethoxysilyl)propyl ammonium chloride (DMOAP) for homeotropic molecular alignment, or coated with polyvinyl alcohol (PVA) and rubbed for homogeneous alignment. The sample temperature was maintained at 25°C. When a constant electric potential with a frequency of 560 kHz was applied, the 514.5-nm linearly polarized laser beam was also normally incident upon the sample. For the homeotropic NLC film, the director always reoriented to the polarization direction of the laser; but for the homogeneous NLC film, as shown in Fig. 1(b), the sample was to be initially aligned such that the rubbing direction was parallel to the polarization direction of the laser, and hence the director could always orient in the y–z plane. When the beam intensity was above a certain threshold value, the transmitted light appeared as a set of conical shells, which form concentric rings on a projection screen. As the number of rings increased or decreased, the half-cone angle of the outermost ring also increased or decreased, respectively. The behavior of the number of rings relative to the electric field and the optical field has been reported in our previous papers.[20–22]

Photographs of the ring structures for the homogeneous NLC film seem almost the same as those for the homeotropic NLC film. Here we show only the photographs for the homeotropic NLC film, but the phenomena for the homogeneous case are also reported. Figures 3(a), 3(b), and 3(c) show the ring structure for the cases when the number of rings is 1, 3, and 9, respectively, where the electric potential $V = 0$. Figures 4(a)–4(c) exhibit the ring structures with the same number of rings as in the preceding case, but under the condition of $V = 2.32$ V. Figures 5(a)–5(c) present the ring structures at $V = 3.68$ V. These photographs are the ring patterns, which are projected normal to a white board with a grid. By comparing the three sets of pictures, we discover some interesting phenomena.

1. For the same number of rings N, it is found that the higher the electric potential, the wider the interval between two rings and the larger the aperture of the far-field ring pattern. Comparing the patterns of $N = 3$, for example, shows that the radius of the outermost ring at $V = 0$ is half that of the outermost ring at $V = 2.32$ V and is one third that at $V = 3.68$ V. In other words, with respect to the same radius, there exist more rings at $V = 0$ than at $V = 2.32$ V and more rings at $V = 2.32$ V than at $V = 3.68$ V. For example, the radius of $N = 9$ at $V = 0$ is close to the radius of $N = 5$ at $V = 2.32$ V and is approximately that of $N = 3$ at $V = 3.68$ V.

2. The second interesting phenomenon is that in every picture the outer rings have the largest bright fringe. The bright-fringe width of the outermost ring not only is the widest but also increases abruptly.

3. Finally, we find that, under the assumption that the ring pattern lies on the x–y plane, the ring structure is symmetric about the y axis but not the x axis when the light polarization is in the y direction. Moreover, for a constant number of rings, the larger the electric field or the optical field, the more asymmetric the ring structure is with respect to the x axis.

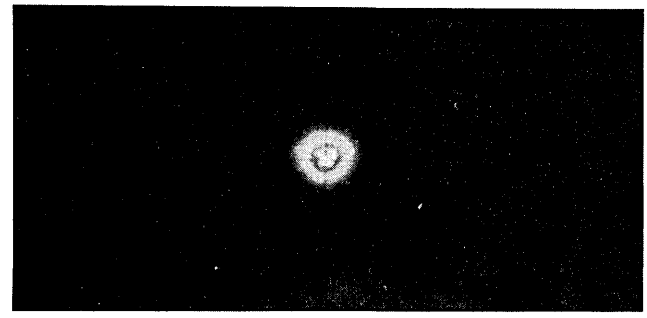

(a)

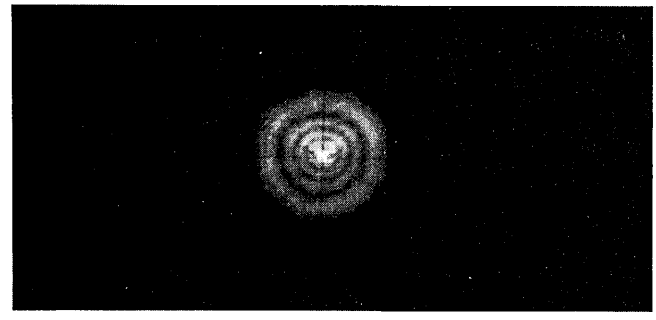

(b)

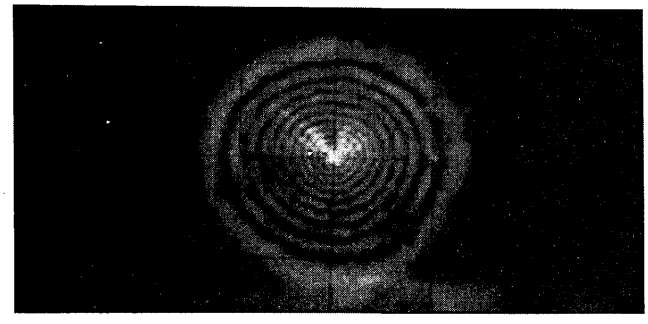

(c)

Fig. 3. For homeotropic ROTN-200, 250-μm film: ring pattern when $V = 0$ V and (a) $N = 1$, (b) $N = 3$, (c) $N = 9$.

4. DISCUSSION

Explanation of Ring Structure

Ring Aperture

In order to give a reasonable explanation for the first phenomenon, the correlation between electrical potential and aperture size, we made some numerical calculation for the homeotropic, 250-μm, ROTN-200 film. For example, we consider a laser beam with a symmetric Gaussian profile of diameter 300 μm and calculate the phase shift induced by different light intensities at zero electric potential (V/V_0 = 0) and a higher electric potential (V/V_0 = 0.6668), by using Eqs. (1), (2), and (6). The material parameters have been reported as $n_\perp = 1.534$, $n_\parallel = 1.795$, $\epsilon_\perp = 7.58$, $\epsilon_\parallel = 8.8$, $k_{11} = 8.284 \times 10^{-7}$ dyn, $k_{33} = 10.033 \times 10^{-7}$ dyn.[20-22] Assuming that there is no nonlocal effect and letting the ring number be 10.5, we plot the wave-front shapes at $V/V_0 = 0$ and at $V/V_0 = 0.6668$ in Fig. 6. From this figure, it can be seen clearly that the wave front at $V/V_0 = 0.6668$ is sharper than that of $V/V_0 = 0$. This implies, from Eq. (9), that the outermost ring radius for $V/V_0 = 0.6668$ is larger than that of $V/V_0 = 0$ and that, furthermore, the larger electric field induces the larger far-field pattern aperture for the same ring number. The physical meaning can be easily comprehended by considering the intensity distribution of the laser beam. The NLC molecule is oriented by the optical field only when the light intensity is higher than the threshold intensity; but the threshold intensity becomes higher when the applied electric field is increased, so that the electric field overcomes the orientation force of the below-threshold optical field. For the sake of simplicity and without numerical calculation, let the induced phase shift vary linearly with intensity when it exceeds the threshold intensity and let the ring number of the two cases be equal. It is then obvious that the distribution of the excess intensity for higher electric potential is sharper than that for lower electric potential when the laser beam diameter is not changed.

We also find something else interesting in Fig. 6. Analyzing the wave-front shapes, we compare each one with the upper part of the related Gaussian-beam intensity profile with an intensity that is higher than the threshold intensity. For $V/V_0 = 0$ and $V/V_0 = 0.6668$, the threshold intensities are $I_{th}/I_0 = 1$ and $I_{th}/I_0 = 1.445$, respectively. We adjust the excess light intensity profile by multiplying times a constant

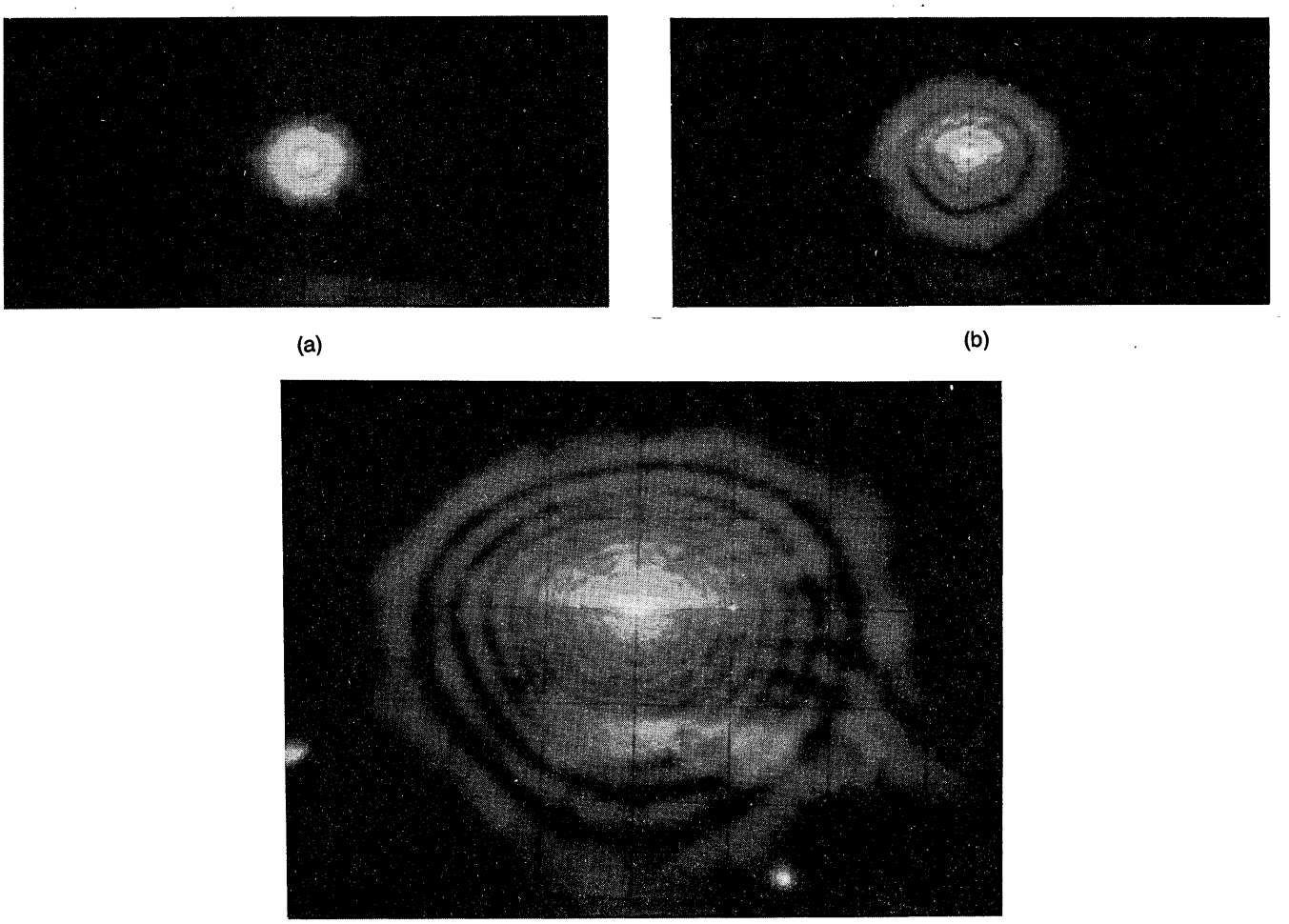

Fig. 4. For homeotropic ROTN-200, 250-μm film: ring pattern when $V = 2.32$ V and (a) $N = 1$, (b) $N = 3$, (c) $N = 9$.

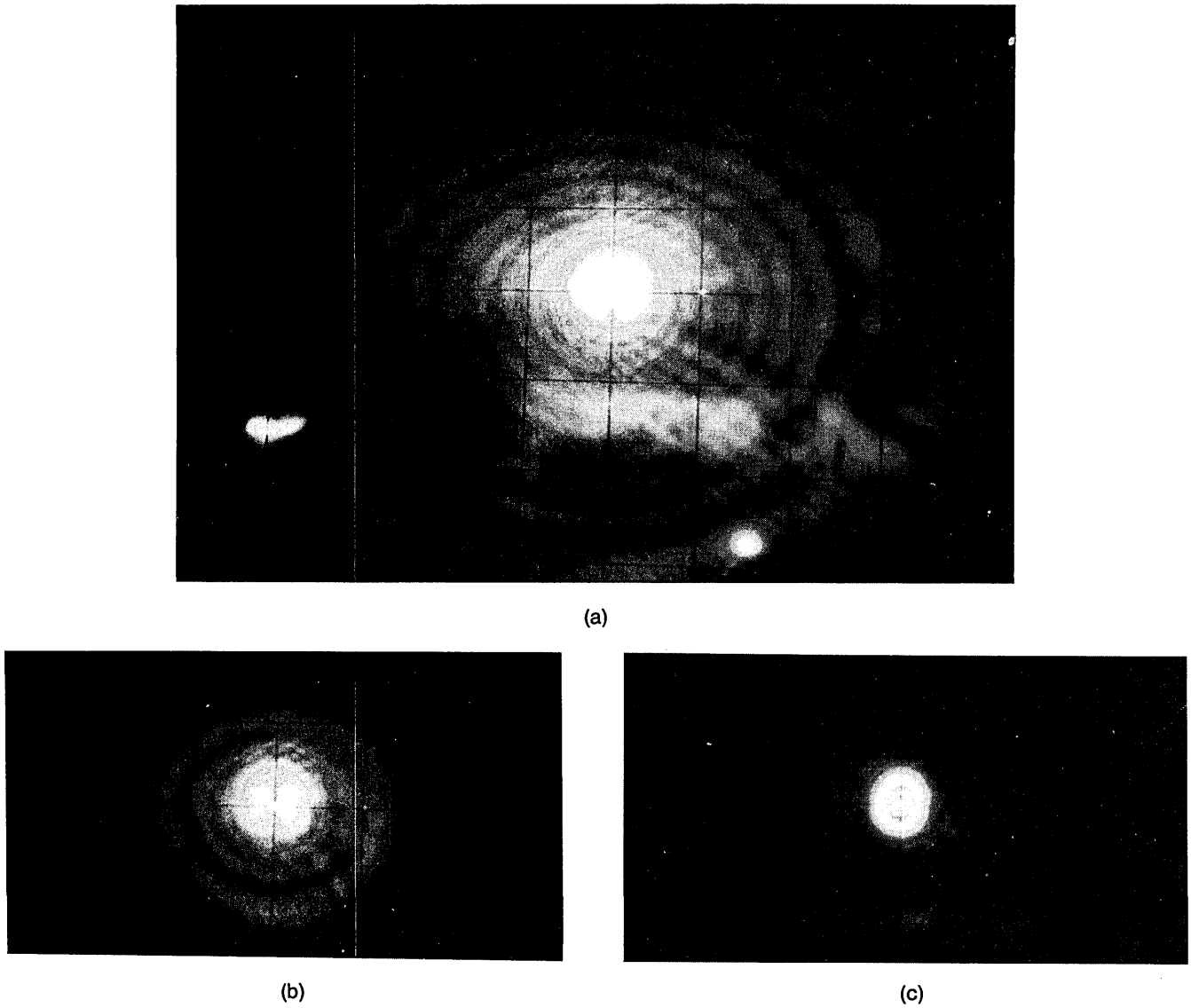

Fig. 5. For homeotropic ROTN-200, 250-μm film: ring pattern, when $V = 3.68$ V and (a) $N = 1$, (b) $N = 3$, (c) $N = 9$.

such that the point of the maximum light intensity is identical to the maximum wave-front deformation profile in Fig. 7(a) and (7b). It is found that with zero electric field and low light intensity, in Fig. 7(a) the wave-front deformation profile is very similar to the distribution profile of the above-threshold intensity. But at a higher-intensity electric field or optical field, in Fig. 7(b) the wave-front deformation profile is higher at the shoulder and sharper at the margin than the distribution profile of the above-threshold intensity. It is then apparent that for a low-intensity external field the deformation of the wave front is almost linear to the excess light intensity, but the deformation is not linear for a higher-intensity external field.

Broadening of Outermost Ring

To explain the second phenomenon, the largest bright fringe on the outermost ring, we give a deeper analysis of the numerical results for the case $V/V_0 = 0.6668$ in Fig. 6. Here

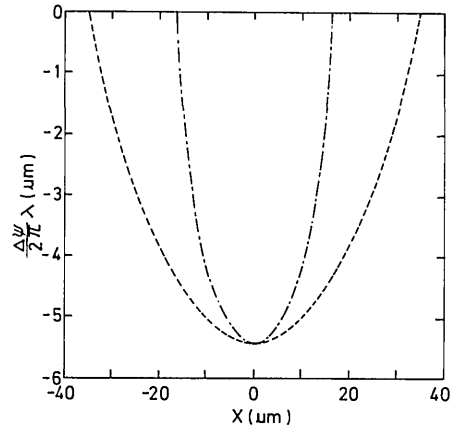

Fig. 6. For homeotropic ROTN-200, 250-μm film: output wave-front shapes of $V/V_0 = 0$ (dashed curve) and $V/V_0 = 0.6668$ (dotted–dashed curve) at $N = 10.5$.

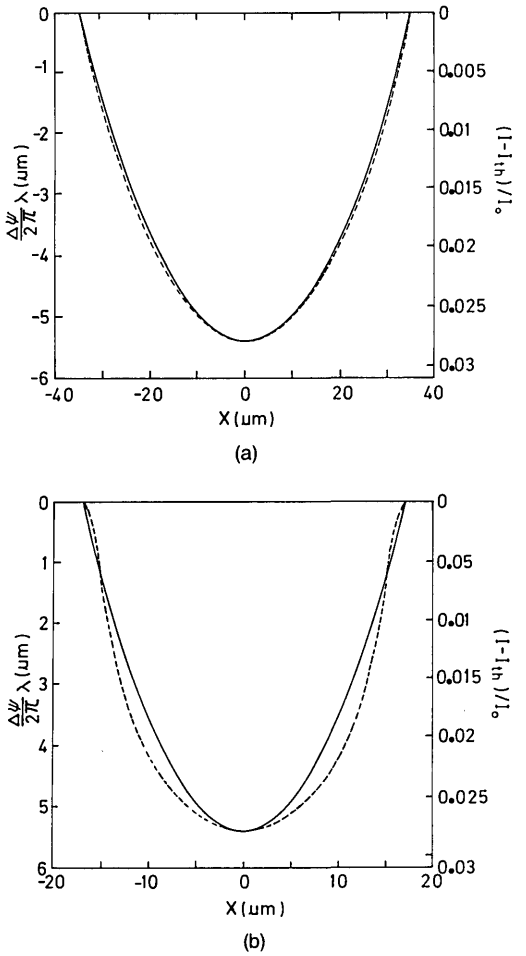

Fig. 7. For homeotropic ROTN-200, 250-μm film: output wave-front profile (dashed curves) and distribution of intensity above threshold (solid curves) at (a) $V/V_0 = 0$, (b) $V/V_0 = 0.6668$.

we mention in passing that the ring pattern is caused by a nonlocal effect. If there is no nonlocal effect, the deformed wave-front profile will have no inflection point, and the absolute value of the slope of the profile will be a simple increasing function of ρ. Under this condition, no two wave vectors will have the same direction and no constructive or destructive interference can occur, as shown in Fig. 2. However, it is very complicated to estimate the nonlocal effect for the molecular reorientation induced by a light beam with Gaussian profile. To simplify this problem, we assume that the nonlocal effect is small and that the inflection point is very close to the margin of the deformed wave-front profile. Under this assumption, rays that come from the deformed wave-front profile should interfere with the rays that come from the inflection point. The outermost ring still comes from the ray with its wave vector perpendicular to the maximum slope. Let $\eta(\rho)$ be the angle between the wave vector and the z axis; let $\varphi(\rho)$ be the phase difference between two rays, one from the deformed wave profile at y and the other from the inflection point. Because the width of the light fringe is proportional to the magnitude of $|d\eta(\rho)/d\varphi(\rho)|$, we calculate $|d\eta(\rho)/d\varphi(\rho)|$ versus y in Fig. 8. It can be seen that the closer to the margin of the deformed wave front, the larger the value of $|d\eta/d\varphi|$. This explains why the outer ring has a larger light band. At the base of the deformed wave-front profile, $|d\eta/d\varphi|$ becomes infinite, and the bright fringe width of the ring should be infinite. But, at this limit, the nonlocal effect is no longer negligible, so that the fringe width does not approach infinity. These are the reasons why the outermost ring abruptly changes such that the light band is approximately twice as wide as the others nearby but is not infinite. To obtain a more precise solution, a much more complicated calculation including the nonfocal effect should be performed.

Asymmetry of Ring

The cause of the third phenomenon, asymmetry about the x axis, is illustrated in Fig. 9. On tracing the rays that pass through the sample film, one finds that rays are deflected in the y–z plane but not in the x–z plane. This means that the ring structure in the far-field pattern is symmetric about the y axis but not about the x axis. This result is reasonable because the incident laser beam is polarized in the y–z plane, and the light reorients NLC molecules only in the y–z plane.

When the laser beam passes through the homeotropic NLC film, the interaction mechanism between light and molecules is as follows. Initially, NLC molecules lie in the z direction. When the laser beam is incident upon the sample

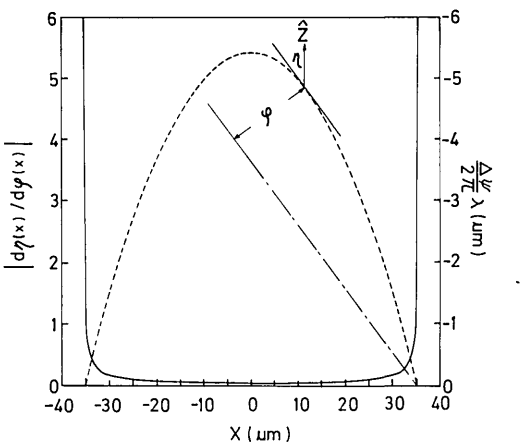

Fig. 8. For homeotropic ROTN-200, 250-μm film: wave-front shape at $V/V_0 = 0$ (dashed curve) and the corresponding value of $|d\eta(\rho)/d\varphi(\rho)|$ (solid curve).

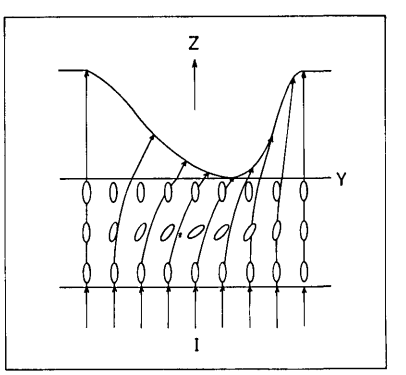

Fig. 9. Rays deflected in the y–z plane when passing through a homeotropic NLC film.

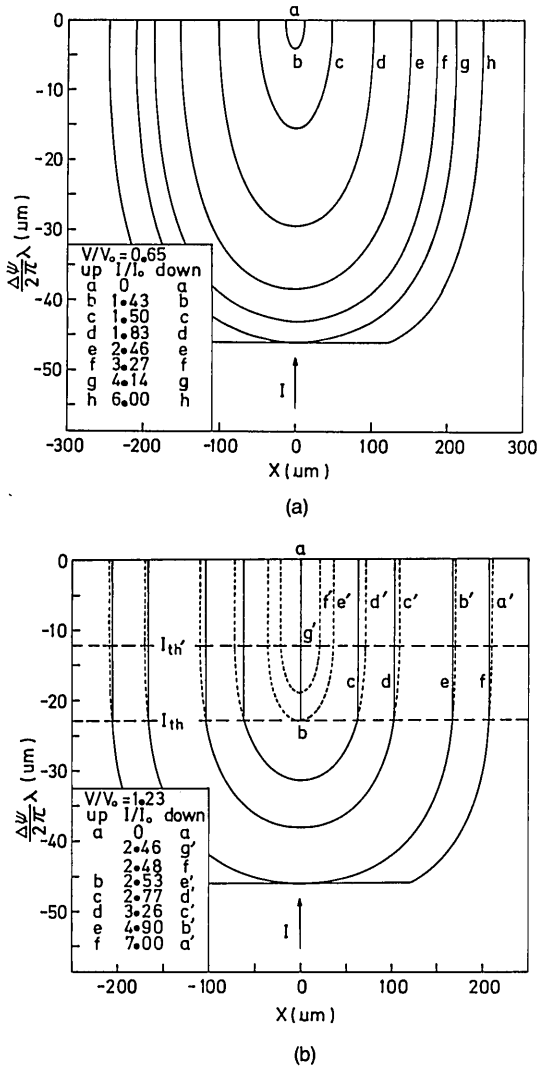

Fig. 10. For homeotropic NLC at fixed electric field and variable optical intensity: (a) $V < V_{Tc}$, second-order Freedericksz transition; (b) $V > V_{Tc}$, first-order Freedericksz transition.

film, the light may reorient NLC molecules to the y axis. Because of the change in the optical axis caused by molecular reorientation, the light should experience a larger refractive index $n(\theta)$ that is nonuniform in the x–y plane and depends on the spatial distribution of the light intensity. The nonuniformity of $n(\theta)$ distorts light rays asymmetrically about the x axis but not about the y axis in the material. In some portions of the beam cross section the light intensity is strengthened, but in other portions the light intensity is weakened, so that the nonuniformity of the light intensity will feed back into the interaction on $n(\theta)$, and so on. Finally, the output wave profile will always be symmetric about the y axis and asymmetric about the x axis. Crudely speaking, the phenomenon results from a nonuniform self-focusing effect. The shape of the wave front should produce two focal points, one on the z axis and the other off the z axis. From the point of view of geometrical optics, this wave-front deformation is not simply astigmatism, i.e., many aberrations also exist. Practically, the sample film is so thin in our experiment that the self-focusing effect is not visible in the material. The observed phenomenon is only the so-called spatial self-phase modulation. From the above explanation, the reason why the third phenomenon occurs is then obvious. Because this phenomenon is caused by the nonuniformity of light, and because light intensity is more nonuniform the larger the electric field or optical field is, the asymmetry of the ring structure is more obvious at a higher-intensity electric field or optical field.

Behavior of the Wavefront—Numerical Analysis

Assuming that there is no nonlocal effect, we can consider in greater detail the distorted wave-front profile output under different optical and electric fields. We analyze by numerical calculation the behavior of the wave-front distortion as a function of a varying electric field with a constant optical field and as a function of a varying optical field with a constant electric field in both homeotropic and homogeneous NLC films. Each one of the four cases becomes two, a second-order and a first-order Freedericksz transition. When the constant electric and optical fields are lower than the tricritical point, only the second-order Freedericksz transition can occur, but when the fields are higher than the

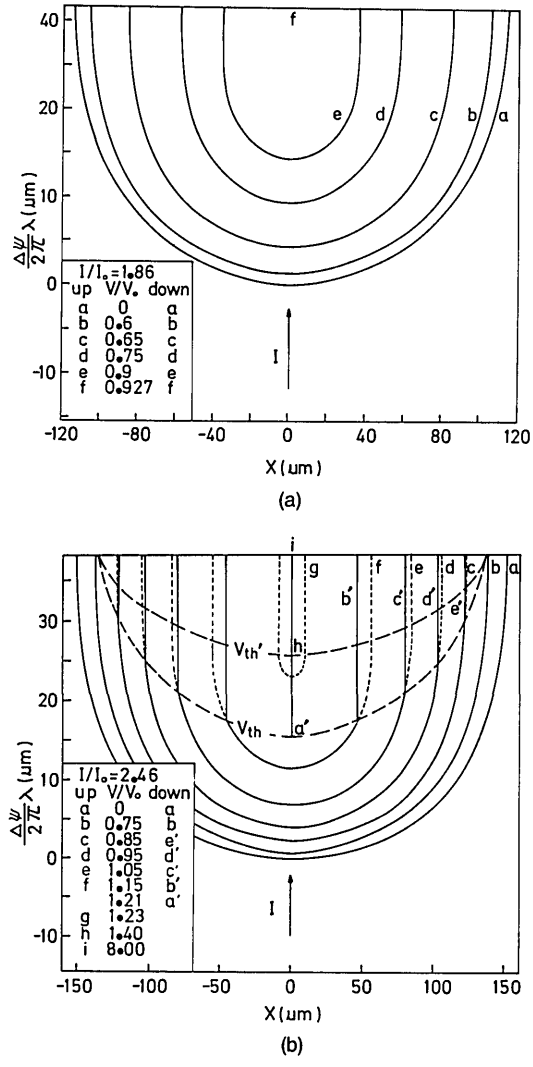

Fig. 11. For homeotropic NLC at fixed optical intensity and variable electric field: (a) $I < I_{Tc}$, second-order Freedericksz transition; (b) $I > I_{Tc}$, first-order Freedericksz transition.

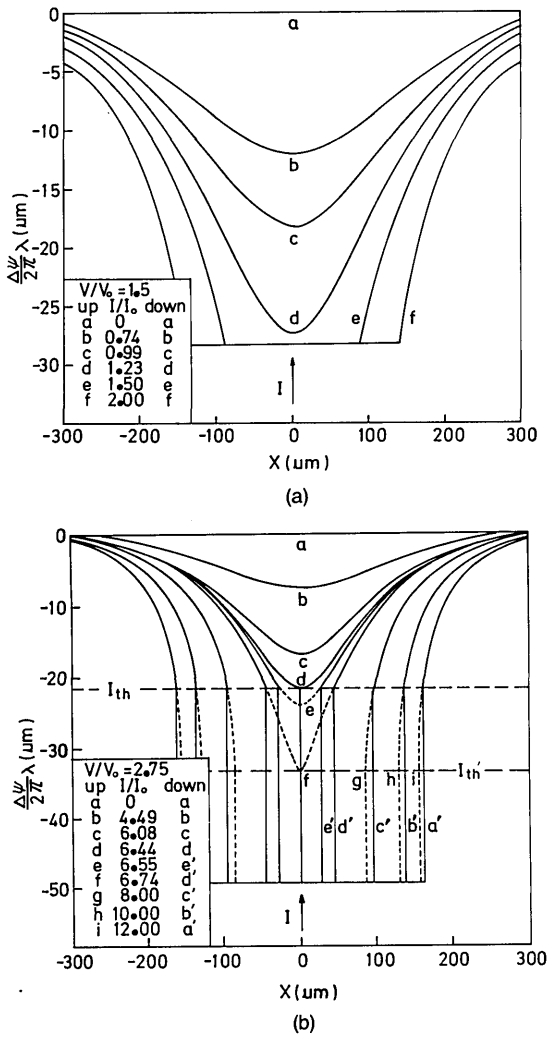

Fig. 12. For homogeneous NLC at fixed electric field and variable optical intensity: (a) $V < V_{Tc}$, second-order Freedericksz transition; (b) $V > V_{Tc}$, first-order Freedericksz transition.

tricritical point, the first-order transition can occur. The numerical results for the wave-front deformation process of the eight cases are plotted in Figs. 10–13. For each figure we set the maximum of the initial deformed wave front to be zero. The incident Gaussian beam diameter is set to be 300 μm, and the thickness of the NLC film is 250 μm.

Figure 10(a) shows the output deformed wave-front profile induced by a fixed electric potential that is lower than the tricritical voltage with a varying optical intensity I from an Ar^+ laser incident in the $+\hat{z}$ direction through the homeotropic NLC film. Under these conditions only second-order molecular reorientation can occur, and there is no first-order transition. When the applied optical intensity is increased, the wave-front retardation will occur in the region where intensity is higher than the threshold intensity. The higher the optical intensity, the more the wave front lags until the intensity reaches the saturation intensity. At this point the valley of the wave-front profile becomes deepest and the number of rings reaches the maximum. If the intensity continues to increase, the number of rings will no longer increase, but the radius will continue to increase. Because there is only a second-order transition, the backward process that decreases the optical intensity makes the number of rings decrease continuously along the path of the forward process. However, when the fixed electric potential V is higher than the tricritical voltage V_{Tc}, a first-order transition occurs. The forward process does not have the same path as the backward process at threshold intensities. The output deformed wave-front profile is shown in Fig. 10(b). In Fig. 10(b) the solid curves represent the deformed wave-front profile at the upward transition, the dashed curves represent the downward transition, and the dashed lines connect the transition points on the deformed wave-front profile. Because of the difference of the upward threshold transition intensity I_{th} and the downward transition intensity I'_{th}, electric-field-induced optical bistability occurs.

Figure 11(a) illustrates the wave-front profile under a second-order molecular reorientation induced by a fixed laser intensity with the maximum optical intensity lower than the tricritical intensity and a varying electric potential in a homeotropic NLC film. Initially, in the absence of an electric field the wave-front retardation is maximum and the

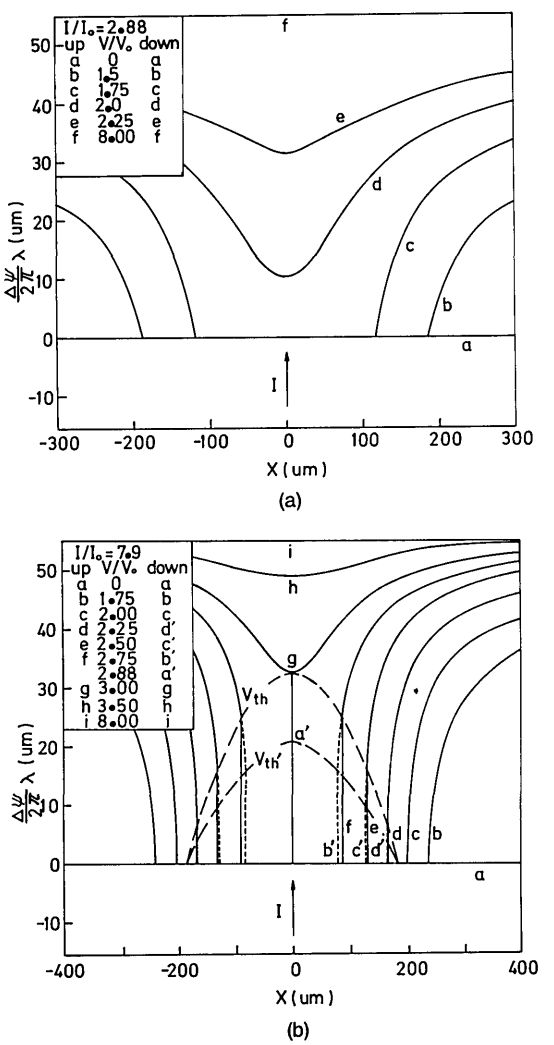

Fig. 13. For homogeneous NLC at fixed optical intensity and variable electric field: (a) $I < I_{Tc}$, second-order Freedericksz transition; (b) $I > I_{Tc}$, first-order Freedericksz transition.

number of rings is the greatest. As the electric field is intensified, the wave front retardation becomes smaller and smaller. Eventually, there is no retardation and there are no rings. Again, since only the second-order transition occurs, the backward process makes the ring number change along the same path as that of the forward process. In Fig. 11(b) we present the profile induced by a fixed laser intensity with a maximum optical intensity higher than the tricritical intensity and a varying electric potential in a homeotropic NLC film. Because of the first-order transition, the forward and backward paths are different at threshold voltages. As the electric field is intensified, the wave-front retardation becomes smaller and smaller, as in the case of Fig. 11(a). However, for some value of the electric potential the first-order transition begins to occur. Above this potential the first-order transition becomes clearer and clearer with increasing voltage until this voltage reaches the downward threshold V'_{th}. At this point the wave front has no deformation. Then, as the electric potential begins to decrease, the first-order Freedericksz transition occurs again at the upward threshold V_{th}. Because $V_{th} \neq V'_{th}$, the optical-field-induced electric bistability occurs.

Figure 12(a) shows the output deformed wave-front profile induced by a fixed electric potential that is lower than the tricritical potential in homogeneous NLC film. At first the electric field is applied such that the NLC molecules are reoriented to the z axis. The electric field is uniform in the sample film, so the molecular reorientation is also uniform. Applying and increasing the optical intensity causes the wave front to begin to be deformed. The higher the optical intensity, the greater the wave front retardation, until the intensity reaches saturation. At this time, as shown in Fig. 10(a), the valley of the wave-front profile becomes deepest and the number of rings reaches the maximum. If the intensity is continuously increased, the radius of the rings will continue to increase and the number of rings will remain constant. Because there is only a second-order transition, the backward path is the same as the forward path. However, as illustrated in Fig. 12(b), in the case in which the initial fixed electric field is higher than the tricritical potential, the first-order Freedericksz transition can occur, and electric-field-induced optical bistability can occur in a homogeneous NLC film. This transition process of the wave-front profile is not the same as that of Fig. 10(b), for the steepest region may be at the margin of the bottom of the deformed wave-front profile when the first-order transition occurs. Then, from Fig. 12(b) we can find that there may exist two inflection points for each side of a deformed wave-front profile. This means that we can simultaneously find two sets of concentric diffraction ring patterns with the same center but with a different period.

Figure 13(a) shows the wave-front profile that is due to second-order molecular reorientation induced by a fixed laser intensity with the maximum optical intensity lower than the tricritical intensity and a varying electric potential in a homogeneous NLC film. Initially, in the absence of an electric field and with only an optical field, there is no wave-front deformation. When the electric field is applied and increased, NLC molecules at the margin of the laser beam begin to reorient to the z axis and the outside wave front begins to lead the inside wave front. The ring number increases until it reaches a maximum. Permitting the electric potential to increase continuously, one will then find that the ring number decreases. When the wave-front deformation vanishes, the ring number will become zero. The backward path is the same as the forward path. At this time the electric field screens out the NLC molecule optical orienting effect. The condition in Fig. 13(b) is almost the same as that in Fig. 13(a). The only difference is that in this case the maximum laser intensity is higher than the tricritical intensity for homogeneous NLC film. Under this condition the first-order Freedericksz transition can occur, and therefore the optical-field-induced electric bistability can exist. Again, as in Fig. 12(b), we may find two inflection points in each side of a deformed wave-front profile. We can also predict the second set of diffraction rings.

5. CONCLUSION

We have investigated both theoretically and experimentally quasi-static electric- and optical-field-induced director reorientation as well as optical wave-front deformation in a NLC film. These studies help to shed light on nonlinear-optical propagation effects such as far-field diffraction rings. It is found that a properly biased quasi-static electric field can enhance or suppress diffraction effects in a NLC film. The enahncement or suppression effect is attributed to the behavior of the NLC above the quasi-static electric-field-induced Freedericksz transition and to nonlinear coupling between the optical and quasi-static electric fields.

In our experiment we have compared the diffraction pattern at different electric potentials and optical intensities. For the same ring number, it was found that the higher the electric potential, the wider the interval between two rings and the larger the aperture of the far-field ring pattern. In other words, the density of the rings is the greatest when there is no electric field. The asymmetry of the diffraction pattern also occurs at a higher electric potential owing to the nonuniformity of the optical intensity. We also found that a second set of diffraction-ring patterns may occur for the first-order Freedericksz transition in homogeneous NLC film. By assuming that there is no nonlocal effect, the deformed wave-front profile was calculated, and the behavior of the deformed wave-front profile can be well described qualitatively. Finally, it is worth mentioning that the nonlocal effect must be considered for more quantitative analysis, though the calculation is much more complicated.

ACKNOWLEDGMENT

This study was supported by the Chinese National Science Council under contract NSC77–0208-M009-02.

REFERENCES

1. R. M. Herman and R. J. Serinko, "Nonlinear-optical processes in nematic liquid crystal near Freedericksz transition," Phys. Rev. A **19**, 1757 (1979).
2. I. C. Khoo, "Optically induced molecular reorientation and third order nonlinear optical processes in nematic liquid crystal," Phys. Rev. A **23**, 2077 (1981).
3. I. C. Khoo, "Nonlinear light scattering by laser- and dc-field-induced molecular orientation in nematic liquid crystal films," Phys Rev. A **25**, 1040, 1636 (1982).
4. P. G. de Gennes, *The Physics of Liquid Crystals* (Clarendon, Oxford, 1974).

5. L. A. Goodman, in *Introduction to Liquid Crystals*, E. B. Priestley, P. J. Wojtowicz, and P. Sheng, eds. (Plenum, New York, 1979), Chap. 14.
6. See, for example, the review paper by I. C. Khoo and Y. R. Shen, "Liquid crystals: nonlinear optical properties and processes," Opt. Eng. **24,** 579 (1985).
7. I. C. Khoo, S. L. Zhuang, and S. Shepard, "Self-focusing of a low power cw laser beam via optically induced birefringence in a nematic liquid crystal film," Appl. Phys. Lett. **39,** 937 (1981).
8. S. D. Durbin, S. M. Arakelian, and Y. R. Shen, "Strong optical diffraction in a nematic liquid crystal with high nonlinearity," Opt. Lett. **7,** 145 (1982).
9. I. C. Khoo, "Optical bistability in nematic films utilizing self-focusing of light," Appl. Phys. Lett. **41,** 909 (1982).
10. N. F. Pilipetski, A. V. Sukhov, N. V. Tabiryan, and B. Ya. Zel'dovich, "The reorientational mechanism of nonlinearity and the self-focusing of He–Ne laser radiation in nematic liquid crystal mesophase (theory and experiment)," Opt. Commun. **37,** 280 (1981).
11. L. Csillag, I. Janossy, V. F. Kitaeva, N. Kroo, N. N. Sobolev, and A. S. Zolotko, "Laser induced reorientation of nematic liquid crystal," Mol. Cryst. Liq. Cryst. **78,** 173 (1981).
12. S. D. Durbin, S. M. Arakelian, and Y. R. Shen, "Laser-induced diffraction rings from a nematic liquid crystal film," Opt. Lett. **6,** 411 (1981).
13. B. Ya, Zel'dovich, N. V. Tabiryan, and Yu. S. Chilingsryan, "Freedericksz transitions induced by light field," Zh. Eksp. Teor. Fiz. **81,** 72 (1981) [Sov. Phys. JETP **54,** 32 (1981)].
14. H. L. Ong, "Optically induced Freedericksz transition and bistability in a nematic liquid crystal," Phys. Rev. A **28,** 2393 (1983).
15. H. L. Ong, "External field enhanced optical bistability in nematic liquid crystal," Appl. Phys. Lett. **46,** 822 (1985).
16. H. L. Ong, "Magnetic-field-enhanced and -suppressed intrinsic optical bistability," Phys. Rev. A **31,** 3450 (1985).
17. H. L. Ong, "Optical-field-enhanced and static-field induced first-order Freedericksz transition in a planar parallel nematic liquid crystal," Phys. Rev. A **33,** 3550 (1986).
18. H. L. Ong, "First and second order Freedericksz transitions in nematic liquid crystal subjected to static and optical-electromagnetic field," IEEE Trans. Electron Devices **ED-25,** 1195 (1986).
19. A. J. Karn, S. M. Arakelian, Y. R. Shen, and H. L. Ong, "Observation of magnetic-field-induced first-order optical Freedericksz transition in a nematic film," Phys. Rev. Lett. **57,** 448 (1986).
20. S.-H. Chen and J. J. Wu, "Observation of first-order Freedericksz transition in a nematic film induced by electric and optical field," Appl. Phys. Lett. **52,** 1998 (1988).
21. J. J. Wu, G. S. Ong, and S.-H. Chen, "Observation of optical-field-induced first-order electric Freedericksz transition and electric bistability in a homogeneous nematic liquid crystal film," Appl. Phys. Lett. **53,** 1999 (1988).
22. J. J. Wu and S-H. Chen, "Optical field induced first order electric Freedericksz transition and electrical bistability in a nematic liquid crystal film," Jpn. J. Appl. Phys. **8,** 429 (1989).
23. C-L. Pan, S-H. Chen, and H. H. Liao, "Quasi-static-electric and optical-field-induced birefringence and nonlinear-optical diffraction effects in a nematic liquid crystal film," Phys. Rev. A **33,** 4312 (1986).
24. L. Csillag, J. Janossy, V. F. Kitaeva, N. Kroo, and N. N. Sobolev, "The influence of finite size of the light spot on the laser introduced reorientation of liquid crystal," Mol. Cryst. Liq. Cryst. **84,** 125 (1982).
25. E. Santamato and Y. R. Shen, "Field-curvature effect on the diffraction ring pattern of a laser beam dressed by spatial self-phase modulation in a nematic film," Opt. Lett. **9,** 564 (1984).
26. I. C. Khoo, T. H. Liu, and P. Y. Yan, "Nonlocal radial dependence of laser-induced molecular reorientation in a nematic liquid crystal: theory and experiment," J. Opt. Soc. Am. B **4,** 115 (1987).
27. I. C. Khoo, J. Y. Hou, T. H. Liu, P. Y. Yan, R. R. Michael, and G. M. Finn, "Transverse self-phase modulation and bistability in the transmission of a laser beam through a nonlinear thin film," J. Opt. Soc. Am. B **4,** 886 (1987).
28. F. Bloisi, L. Vicari, F. Simoni, G. Cipparrone, and C. Umeton, "Self-phase modulation in nematic liquid-crystal films: detailed measurements and theoretical calculations," J. Opt. Soc. Am. B **5,** 2462 (1988).